

Is the $\text{Yb}_2\text{Ti}_2\text{O}_7$ pyrochlore a quantum spin ice?

R. Applegate,¹ N. R. Hayre,¹ R. R. P. Singh,¹ T. Lin,² A. G. R. Day,^{2,3} and M. J. P. Gingras^{1,2,4}

¹Physics Department, University of California at Davis, Davis, CA 95616

²Department of Physics and Astronomy, University of Waterloo, Waterloo, Ontario, N2L 3G1, Canada

³Département de Physique, Université de Sherbrooke, Sherbrooke, Québec, J1L 2R1, Canada

⁴Canadian Institute for Advanced Research, 180 Dundas St. W., Toronto, Ontario, M5G 1Z8, Canada

(Dated: September 2, 2018)

We use numerical linked cluster (NLC) expansions to compute the specific heat, $C(T)$, and entropy, $S(T)$, of a quantum spin ice model of $\text{Yb}_2\text{Ti}_2\text{O}_7$ using anisotropic exchange interactions recently determined from inelastic neutron scattering measurements and find good agreement with experimental calorimetric data. In the perturbative weak quantum regime, this model has a ferrimagnetic ordered ground state, with two peaks in $C(T)$: a Schottky anomaly signalling the paramagnetic to spin ice crossover followed at lower temperature by a sharp peak accompanying a first order phase transition to the ferrimagnetic state. We suggest that the two $C(T)$ features observed in $\text{Yb}_2\text{Ti}_2\text{O}_7$ are associated with the same physics. Spin excitations in this regime consist of weakly confined spinon-antispinon pairs. We suggest that conventional ground state with exotic quantum dynamics will prove a prevalent characteristic of many real quantum spin ice materials.

PACS numbers: 74.70.-b, 75.10.Jm, 75.40.Gb, 75.30.Ds

The experimental search for quantum spin liquids (QSLs), magnetic systems disordered by large quantum fluctuations, has remained unabated for over twenty years [1]. One direction that is rapidly gathering momentum is the search for QSLs among materials that are close relatives to spin ice systems [2], but with additional quantum fluctuations, or *quantum spin ice* [3, 4].

Spin ices are found among insulating pyrochlore oxides, such as $\text{R}_2\text{M}_2\text{O}_7$ ($\text{R}=\text{Ho}, \text{Dy}$; $\text{M}=\text{Ti}, \text{Sn}$) [5]. In these compounds, the magnetic R rare earth ions sit on a lattice of corner-sharing tetrahedra, experiencing a large single-ion anisotropy forcing the magnetic moment to point strictly “in” or “out” of the two tetrahedra it joins (see Fig. 1a). Consequently, the direction of a moment can be described by a classical Ising spin [2]. In these materials, the combination of nearest-neighbor exchange and long-range magnetostatic dipolar interactions lead to an exponentially large number of low-energy states characterized by two spins pointing in and two spins pointing out on each tetrahedron (see Fig. 1a). This energetic constraint is equivalent to the Bernal-Fowler ice rule which gives water ice a residual entropy $S_{\text{P}} \sim k_{\text{B}}(\frac{1}{2}) \ln(3/2)$ per proton, estimated by Pauling [6] and in good agreement with experiments on water ice [7]. Since they share the same “ice-rule”, the $(\text{Ho}, \text{Dy})_2(\text{Ti}, \text{Sn})_2\text{O}_7$ pyrochlores also possess a residual low-temperature Pauling entropy S_{P} [8], hence the name spin ice. The spin ice state is not thermodynamically distinct from the paramagnetic phase. Yet, because of the ice-rules, it is a strongly correlated state of matter – a *classical* spin liquid of sorts [1, 2].

For infinite Ising anisotropy, quantum effects are absent [2]. However, these can be restored when considering the realistic situation of *finite* anisotropy. In two closely related papers, Hermele *et al.* [9] and Castro-Neto *et al.* [10] considered effective spins one-half on a py-

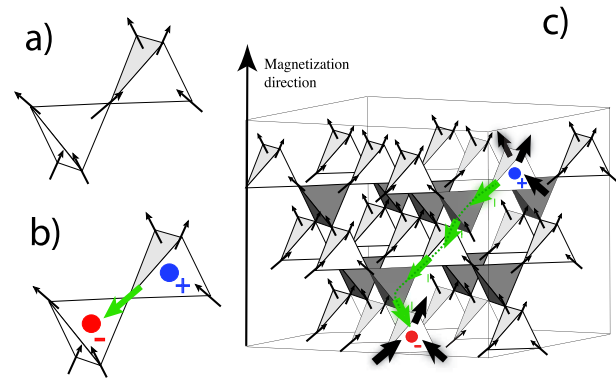


FIG. 1: (a) Two neighboring tetrahedra with spins in their two-in/two-out ground state, (b) spinon/antispinon pair, (c) spinon/antispinon pair separated by a (green) string of misaligned spins in the pyrochlore lattice.

rochlore lattice where the highly degenerate classical spin ice state is promoted via quantum fluctuations to a QSL with fascinating properties. This QSL is described by a compact lattice quantum electrodynamics (QED) -like theory. In this QSL state inherited from the parent classical spin ice, the ice-rules amount to a divergence-free coarse-grained fictitious electric field whose sources are deconfined spinons while the sources of the canonically conjugate field are deconfined monopoles [11], along with a gauge boson (“artificial photon”).

Recent numerical studies have found evidence that QED-like phenomena may be at play in some minimal quantum spin ice (QSI) lattice models [13] – but does the QSI picture apply to real materials? Also, should a QSI state be solely defined by whether or not a QSL state is realized? While a QSI picture has been suggested relevant to the QSL behavior in $\text{Tb}_2\text{Ti}_2\text{O}_7$ [3]

and $\text{Pr}_2\text{M}_2\text{O}_7$ [4], intense experimental [14–21] and theoretical [16–18, 21–26] interest has recently turned to $\text{Yb}_2\text{Ti}_2\text{O}_7$ (YbTO), which has been argued to be on the verge of realizing a QSL originating from QSI physics. In fact, the combination of (i) an unexplained transition at $T_c \sim 0.24$ K [14, 27], (ii) the controversial evidence for long-range order below T_c [28, 29] and (iii) the high sensitivity of the low-temperature ($T < 300$ mK) behavior to sample preparation conditions [19, 20] are all tantalizing evidence that YbTO has a fragile and perhaps unconventional ground state. Thus, explaining YbTO is a key milestone in the study of QSI in a materials context.

In this paper, we first use the numerical linked cluster (NLC) method [30, 31] to calculate the heat capacity, $C(T)$, and entropy, $S(T)$, of a microscopic model for YbTO with exchange parameters, $\{J_e\}$, taken from Ref. [18]. This calculation, which converges down to about 1 K, agrees well with experiments. It demonstrates that YbTO is indeed a spin-half, anisotropic exchange model, with $\{J_e\}$ determined from magnon energies in the strong-field polarized paramagnet regime [18]. Our work suggests that a two-peaked $C(T)$ structure is natural in YbTO and should be present in the best (“quality”) samples [19, 20]. Below the higher temperature $C(T)$ hump near 2 K, the system has a residual $S(T)$ comparable to S_P , but without a clean $S(T) \approx S_P$ plateau developing upon cooling. We propose that the lower temperature sharp peak in $C(T)$ is associated with a strongly first order transition to a ferrimagnetic state. Such a behavior is indeed found in our study when the quantum (non-Ising) exchanges are small. Finally, we argue that despite a conventional ground state, the spin excitations consist of spinon/antispinon pairs connected with (Dirac-like [12]) strings of reversed spins, whose confinement length l_s diverges in the limit of small quantum exchanges. We propose that these excitations should ultimately form the basis for describing what we expect to be highly unconventional inelastic neutron spectra [26].

Model & Method – The anisotropic exchange QSI model is defined by the nearest-neighbor Hamiltonian [18, 25] on the pyrochlore lattice

$$\begin{aligned} \mathcal{H}_{\text{QSI}} = & \sum_{\langle i,j \rangle} \{J_{zz} S_i^z S_j^z - \lambda J_{\pm}(S_i^+ S_j^- + S_i^- S_j^+) \\ & + \lambda J_{\pm\pm} [\gamma_{ij} S_i^+ S_j^+ + \gamma_{ij}^* S_i^- S_j^-] \\ & + \lambda J_{z\pm} [(S_i^z (\zeta_{ij} S_j^+ + \zeta_{i,j}^* S_j^-) + i \leftrightarrow j)]\}. \end{aligned} \quad (1)$$

γ_{ij} is a 4×4 complex unimodular matrix, and $\zeta = -\gamma^*$ [18]. The \hat{z} quantization axis is along the local [111] direction, and \pm refers to the two orthogonal local directions. We take $\lambda = 1$, except when stated otherwise.

Recently Ross *et al.* [18] used inelastic neutron scattering data in high fields to deduce the $\{J_e\}$ exchange parameters for YbTO: $J_{zz} = 0.166 \pm 0.04$, $J_{\pm} = 0.05 \pm 0.01$, $J_{\pm\pm} = 0.05 \pm 0.01$, and $J_{z\pm} = -0.14 \pm 0.01$, all in meV. These parameters have also been determined through an

analysis of the zero-field energy-integrated paramagnetic neutron scattering [17, 21], but the values of the $\{J_e\}$ parameters disagree significantly – an issue that we address in the supplementary material [32].

NLC expansions provide a controlled way of calculating macroscopic properties of a thermodynamic system [30, 31]. By summing up contributions from clusters up to some size, one can obtain properties in the thermodynamic limit, which include all terms in high temperature expansions up to some order. Furthermore, since the contributions of the clusters are entirely included for all temperatures, all short distance physics is fully incorporated, and thus can converge down to lower temperatures than a (high-temperature, T) series expansion [30] in $1/T$. NLC is particularly suited to the study of spin ice systems. It was recently shown that for classical spin ice models, just first order NLC based on a single tetrahedron, gives $C(T)$ and $S(T)$ for all T within a few percent accuracy [33].

Here, we calculate the thermodynamic properties of the exchange QSI model of Eq. (6) using tetrahedra-based NLC up to 4th order [32]. Euler extrapolations [34] are used to eliminate some alternating pieces in the expansion, which further improves the convergence of the calculations to lower T . In zero field, there is only one cluster in each of the first three orders, and three clusters in the fourth order [32]. The different g -tensor elements on different sites (expressed in a global frame) [24] mean that many more clusters are needed for calculating field-dependent $C(T)$, magnetization and susceptibility, and these will be presented elsewhere.

Figure 2 shows $C(T)$ calculated with different NLC orders. By 4th order, there is good convergence to temperatures below the $C(T)$ peak at ~ 2 K. Applying Euler transformations [34] improves the convergence down to slightly below 1 K. The experimental data from Refs. [27], shown for comparison, agree well with the NLC results. Here, we used the mean values of the $\{J_e\}$ from Ref. [18] and did not adjust any parameters. Given the variability in the experimental $C(T)$ data from one group to another [19–21, 32], it does not seem useful at this time to search for $\{J_e\}$ parameters giving a better fit. This agreement shows that the $\{J_e\}$ parameters are not substantially renormalized compared to the high (5 Tesla) field values [18]. Using the $\{J_e\}$ of Refs. [17, 21] gives substantially different $C(T)$ results [32].

Figure 3 shows $S(T)$ calculated by NLC, together with the entropy obtained by integrating $C(T)/T$ data of Ref. [27]. We found the data from Ref. [27] ideally suited to perform this comparison [32]. The entropy converges to lower temperature slightly better than $C(T)$ where, with Euler transformations, $S(T)$ converges down to about 0.7 K, matching well with the experimental entropy values over the overlapping temperature range.

Perturbative considerations – In order to better understand the properties of this system, we turn to the perturbative regime $\lambda \ll 1$ in Eq. 1 [18, 25]. To second

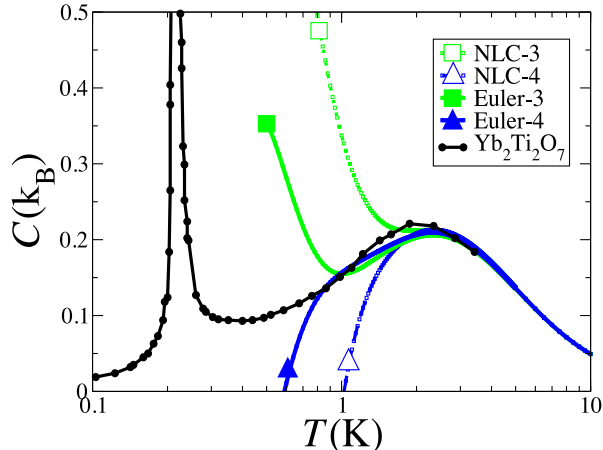


FIG. 2: Specific heat, $C(T)$, per mole of Yb for the model parameters in Ref. [18], in units of the Boltzmann constant k_B , calculated via NLC (up to 4th order NLC together with Euler extrapolations) are compared with experimental data for $\text{Yb}_2\text{Ti}_2\text{O}_7$. The black circles are data from Ref. [27].

order in λ , only $J_{z\pm}$, by far the largest quantum term for YbTO, leads to a degeneracy-lifting classical potential for different spin-ice configurations. It amounts to a fluctuation-induced ferromagnetic exchange constant $J_3 \equiv -3\lambda^2 J_{z\pm}^2 / J_{zz}$ [25] between shortest distance spins on the same tetrahedral sublattice that share a neighbor [35]. It leads to the selection of a $\mathbf{q} = 0$ long-range ordered ground state in which all tetrahedra are in the same configuration and the spins develop a small ferromagnetic moment along one of the $\langle 100 \rangle$ cubic directions. This $\mathbf{q} = 0$ ferrimagnet (FM) lacks the Coulombic physics originally present in the J_{zz} -only spin ice model [36].

To calculate $C(T)$ and $S(T)$ in the perturbative regime at low T , we turn to classical loop Monte Carlo simulations [37] of the $J_3 - J_{zz}$ model [32]. These reveal a very sharp lower temperature peak signalling a first order phase transition to a $\mathbf{q} = 0$ state (see Fig. S5 [32]).

Excited states in the perturbative regime: spinons and strings – A surprise of the perturbative treatment is that, while the ground state is classical, the spin-flip excitations remain non-trivial and of quantum nature. This is because, once a spin is flipped in a spin-ice state, creating a spinon/antispinon pair [11], the pair can hop through $J_{z\pm}$ acting through *first order* degenerate perturbation theory. Thus, the dispersion in the excited state manifold is $\lambda J_{z\pm}$, *much larger* than the dispersion within the low-energy manifold of spin ice states, which is only $\lambda^2 J_{z\pm}^2 / J_{zz}$.

A sketch of a spinon/antispinon pair is shown in Fig. 1b and 1c. Note that only spins inside the tetrahedron “already” containing spinons are flippable in first order

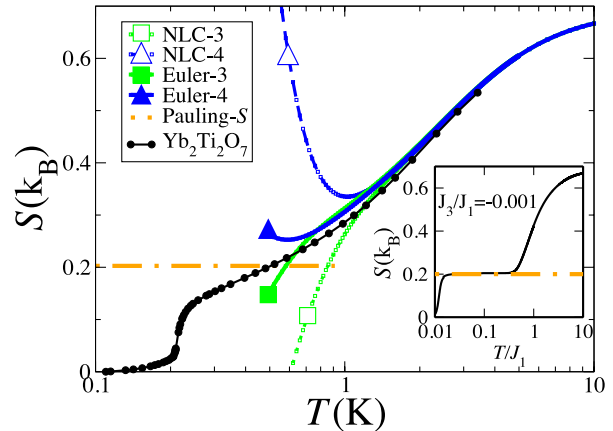


FIG. 3: Entropy, $S(T)$, per mole of Yb, in units k_B following the methods described in the caption of Fig. 2. The black circles are obtained by integrating the data from Ref. [27] excluding the nuclear (hyperfine) contribution. The Pauling entropy $S_P \sim \frac{k_B}{2} \ln \frac{3}{2}$ is shown as a horizontal line. The inset shows $S(T)$ in the perturbative regime with $J_3/J_{zz} = -0.001$. A clear plateau at $S(T) \approx S_P$ is seen, followed at lower T by a precipitous drop of $S(T)$ (i.e. latent heat) accompanying the transition to long range FM order [32].

degenerate perturbation theory. Hence, the connecting string of misaligned spins can only fluctuate by higher order processes involving closed loops with alternating in-out spins [26]. Thus the renormalized string tension per unit length remains finite and of order J_3 . One can estimate the typical string length as the length, l_s , at which the cost of the string becomes comparable to the delocalization energy of the spinon/antispinon pair. The string energy per unit length goes as $\sim J_3 \sim \lambda^2$, whereas the delocalization energy (spinon bandwidth) goes as λ . This leads to l_s scaling as $1/\lambda$, which diverges as $\lambda \rightarrow 0$.

A detailed theory of neutron scattering in this ferrimagnetic phase is not attempted here, but we anticipate it to follow the proposal of Ref. [26]. At temperatures above the transition to the $\mathbf{q} = 0$ long-range ordered state, the system explores the classical two-in/two-out spin ice states and should display singularities (pinch points, PPs) in neutron scattering [36] rounded off by the finite density of thermally excited spinon/antispinon defects [11, 36]. While the system has thermally smeared PPs above the ferrimagnetic transition and no static PPs well below the transition, it may display some remnant of PPs in the spin dynamics at higher energies. These interesting issues deserve further attention.

Beyond the $\lambda \ll 1$ regime – Why is the transition temperature of YbTO so low? As discussed by Ross *et al.* [18], the low T peak in $C(T)$ is at a temperature lower than mean-field theory by an order of magnitude. Com-

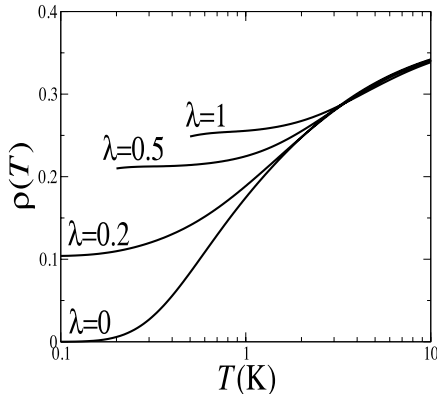


FIG. 4: Monopole defect density, $\rho(T)$, calculated using NLC, shown down to a temperature where 3rd and 4th order Euler Transforms agree. Here, quantum exchanges are scaled with respect to YbTO parameters by different values of λ .

paring $C(T)$ for the quantum model with different λ with the corresponding classical model with the perturbative J_3/J_{zz} value provides a hint of the reason why [32]. It shows that, in the classical model, the long-range order keeps steadily moving up with increased J_3 , even beyond the short-range order $C(T)$ peak. In contrast, the quantum systems, with different λ continue to display a short-range order $C(T)$ peak and presumably long-range order only occurs at a much lower T . Perturbative considerations here have an analogy with strong coupling studies of Mott physics in the Hubbard model, where the Néel temperature first increases with t as t^2/U but then begins decreasing when the system moves away from the perturbative small t/U regime. We propose that a similar non-monotonic T_c arises in this QSI model due to enhanced quantum fluctuations.

Another argument for a reduced T_c comes from considering the temperature dependence of the defect (spinon/antispinon) monopole density, $\rho(T)$, as calculated by NLC (see Fig. 4 and Figs. S3 and S4 [32]). To illustrate the point, we show the behavior for several different λ values. Convergence increases to lower T , with decreasing λ , as expected. One finds that as T drops below the hump in $C(T)$, $\rho(T)$ displays a plateau-like region, whose value increases steadily with increasing λ . This indicates that the states *within* the spin-ice manifold develop large spinon/antispinon spectral weight, thus strongly renormalizing all low energy scales and, presumably, leading to reduced T_c .

Discussion: What constitutes an exchange QSI? – We suggest that a double-peaked $C(T)$ with an entropy between the peaks comparable to S_P is the hallmark of an exchange quantum spin ice (QSI). However, one is unlikely to find an exact plateau at $S(T) \approx$

S_P outside the perturbative (small λ) regime. Such a double-peaked structure and quasi-separation of the energy/temperature scales associated with short and long-range physics has also been suggested for other systems where quantum spin liquid physics may apply [38].

According to the gauge mean-field theory of Ref. [25], at low temperature below which short-range spin ice correlations develop, a system may exhibit either a conventional ferrimagnetic (FM) order, a Coulombic ferromagnet (CFM) or a full-blown quantum spin-liquid (QSL), depending on its quantum exchange parameters. The largest quantum exchange terms in YbTO is $J_{z\pm}$, which favors the FM state, which we believe is the origin of the 0.24 K transition in the best samples [28]. It remains to be seen if there are real materials for which J_{\pm} , which favors the QSL [9, 10, 25], is the dominant quantum term. Nevertheless, even when the ground state is FM, the excitations remain highly exotic, consisting of spinon-antispinon pairs separated by long strings. This non-trivial feature is derived from the underlying spin-ice physics. Finally, as one notes that $J_{z\pm}$ is strictly zero for non-Kramers ions (e.g. Pr, Tb) and that virtual crystal field excitations [3] in Tb-based pyrochlores are a fundamentally different pathway from anisotropic superexchange [4] to generate anisotropic $\{J_e\}$ couplings between effective spins one-half [3, 4], the prospect to ultimately find a QSI-based QSL among rare-earth pyrochlores [5] is perhaps promising.

This work is supported in part by NSF grant number DMR-1004231, the NSERC of Canada and the Canada Research Chair program (M.G., Tier 1). We acknowledge very useful discussions with B. Javanparast, K. Ross and J. Thompson. We thank P. Dalmas de Réotier for providing specific heat data of Ref. [19].

Supplementary Material

This supplement provides the reader with further material to assist with some of the technical materials of the main part paper

Numerical Linked Cluster Method

For the proposed QSI Hamiltonian [18], the numerical linked cluster (NLC) method [30, 31] gives reliable quantitative properties of the system in the thermodynamic limit down to some temperature by developing an expansion in connected tetrahedra that embed in the pyrochlore lattice. For each cluster, we perform an exact diagonalization (ED) and calculate physical quantities from the resulting spectrum and states. Once a property is calculated, the properties of all subclusters are subtracted to get the weight of the cluster c denoted as

$W(c)$. In the thermodynamic limit, an extensive property, P is expressed as

$$P/N = \sum_c L(c) \times W(c), \quad (2)$$

where L_c is the count of the cluster, per lattice site.

We consider all clusters up to four tetrahedra, the largest diagonalization being a 13-site system. All states are required to calculate the partition function and thermodynamic quantities presented below. The particular clusters to fourth order in our expansion are shown in Figure S1.

Computational Requirements

NLC using the tetrahedral basis requires exact diagonalization of increasingly large tetrahedral clusters. Using modern hardware and freely-available linear algebra routines, diagonalizations for clusters of one tetrahedron (four sites) and two tetrahedra (seven sites) could be done in less than a second, while the three-tetrahedron (10-site) cluster still required less than 10 seconds. Computing only the spectrum for a single four-tetrahedron (13-site) cluster required about 1200 seconds and more than 1 GB of memory, while generating the full set of eigenstates required approximately 8 GB of memory. Note that the Hamiltonian of an N -site cluster is a $2^N \times 2^N$ complex Hermitian matrix. Exact diagonalizations of larger systems are, in practice, limited by memory requirements. The next order calculation will have 3 more sites and the memory requirement will grow by a factor of 64.

Euler Summation

NLC generates a sequence of property estimates $\{P_n\}$ with increasing order n , where $P_n = \sum_{i=1}^n S_i$ and S_i is some physical quantity calculated at the i th order. When such a sequence is found to alternate, its convergence can be improved by Euler Transformation [34]. In general, given alternating terms $S_i = (-1)^i u_i$, the Euler Transform method amounts to estimates,

$$u_0 - u_1 + u_2 - \dots - u_{n-1} + \sum_{s=0} \frac{(-1)^s}{2^{s+1}} [\Delta^s u_n], \quad (3)$$

where Δ is the forward difference operator

$$\begin{aligned} \Delta^0 u_n &= u_n, \\ \Delta^1 u_n &= u_{n+1} - u_n, \\ \Delta^2 u_n &= u_{n+2} - 2u_{n+1} + u_n, \\ \Delta^3 u_n &= u_{n+3} - 3u_{n+2} + 3u_{n+1} - u_n, \dots \end{aligned} \quad (4)$$

Usually, a small number of terms are computed directly, and the Euler transformation is applied to rest of the

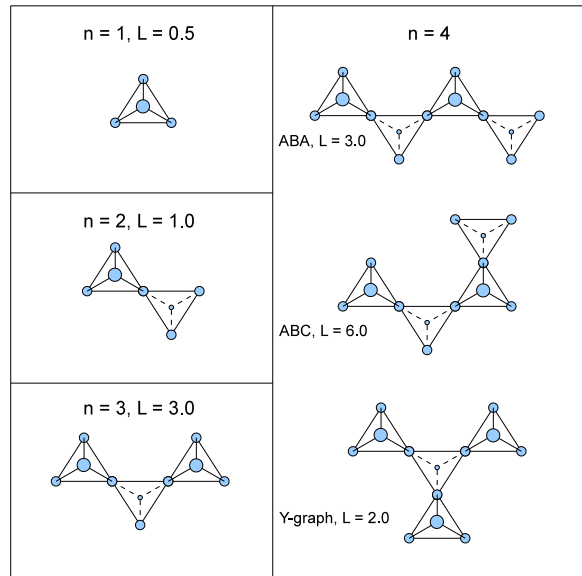


FIG. 5: S1: Clusters used for the zero-field NLC expansion in the tetrahedral basis, up to fourth order. Each graph is accompanied by its lattice constant L .

series. In our case, where direct terms are available to fourth order, we begin the Euler transform after the second order, so that the third and fourth order Euler-transformed property estimates are

$$\begin{aligned} P_{3,E} &= S_0 + S_1 + S_2 + \frac{1}{2}S_3, \\ P_{4,E} &= P_{3,E} + \frac{S_3 + S_4}{4}. \end{aligned} \quad (5)$$

Various Hamiltonians and perturbative limit

We use the notation of Ross *et al.* [18] and define the quantum spin ice Hamiltonian as

$$\begin{aligned} \mathcal{H}_{\text{QSI}} &= \sum_{\langle i,j \rangle} \{J_{zz} S_i^z S_j^z - J_{\pm} (S_i^+ S_j^- + S_i^- S_j^+) \\ &\quad + J_{\pm\pm} [\gamma_{ij} S_i^+ S_j^+ + \gamma_{ij}^* S_i^- S_j^-] \\ &\quad + J_{z\pm} [(S_i^z (\zeta_{ij} S_j^+ + \zeta_{i,j}^* S_j^-) + i \leftrightarrow j)]\}. \end{aligned} \quad (6)$$

The parameters for $\text{Yb}_2\text{Ti}_2\text{O}_7$ determined by fitting from high-field inelastic neutron (magnon) spectra in Ref. [18] are, measured in meV, $J_{zz} = 0.166 \pm 0.04$, $J_{\pm} = 0.05 \pm 0.01$, $J_{\pm\pm} = 0.05 \pm 0.01$, and $J_{z\pm} = -0.14 \pm 0.01$. Two other sets of parameter estimates for $\text{Yb}_2\text{Ti}_2\text{O}_7$ were determined by fitting the diffused (energy-integrated) neutron scattering using the random phase approximation (RPA) [17, 21]. The values obtained by Thompson *et al.* [17] are: $J_{zz} = 0.023$, $J_{\pm} = 0.038$, $J_{\pm\pm} = 0.007$, and $J_{z\pm} = -0.040$, while those obtained by Chang *et*

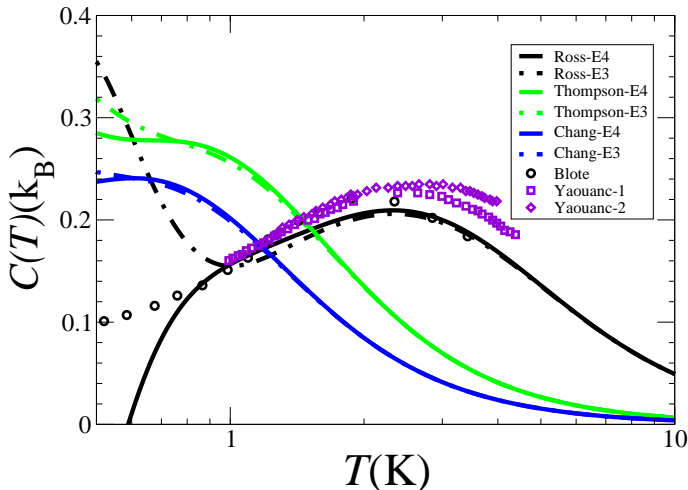


FIG. 6: S2: Molar heat capacity for YbTO reported by Blöte *et al.* [27] and by Yaouanc *et al.* [19] compared with calculated values using exchange parameters from Ross *et al.* (Ross-E3,E4) [20], Thompson *et al.* (Thompson-E3,E4) [17] and Chang *et al.* (Chang-E3,E4) [21]. Third (E3) and Fourth (E4) order Euler Transforms of the NLC results using the parameters are shown.

al. [21] are $J_{zz} = 0.059$, $J_{\pm} = 0.023$, $J_{\pm\pm} = 0.006$, and $J_{z\pm} = -0.029$. In all cases, the values of the $\{J_e\}$ exchange parameters are given in meV. The calculated heat capacity for all these parameters, together with the experimental data on $\text{Yb}_2\text{Ti}_2\text{O}_7$ from difference groups [19, 20], are shown in Fig. S2. It is clear that the latter two parametrizations by Thompson *et al.* and Chang *et al.* do not give a good description of the heat capacity of the material. It is not clear at this time why RPA calculations find such $\{J_e\}$ parameters compared to high-field paramagnon spectra [20]. This problem warrants further attention.

In order to explore to what extent quantum mechanical effects are at play in \mathcal{H}_{QSI} , we introduce a Hamiltonian with rescaled quantum terms as

$$\mathcal{H}_\lambda = \mathcal{H}_0 + \lambda\mathcal{H}_1, \quad (7)$$

where \mathcal{H}_0 is the classical spin-ice Hamiltonian consisting of J_{zz} terms only, while all other terms are included in \mathcal{H}_1 . The value $\lambda = 1$ corresponds to the parameters of Ross *et al.*[18] In the perturbative regime ($\lambda \ll 1$), this model maps on to a $J_1 - J_3$ model with $J_1 = J_{zz}$ and $J_3 = -3\lambda^2 J_{z\pm}^2 / J_{zz}$.

Specific heat and entropy of the system with different values of λ in 4th order Euler Transform, down to a temperature where 3rd and 4th order Euler Transforms agree with each other are shown in Fig. S3 and Fig. S4. Heat capacity of the perturbative classical $J_1 - J_3$ model, calculated by classical loop Monte Carlo simulations [37] is

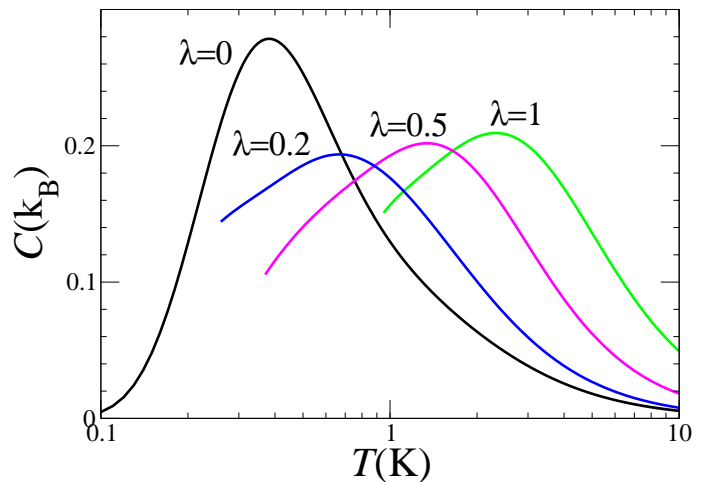


FIG. 7: S3: Heat capacity where quantum terms are scaled by λ .

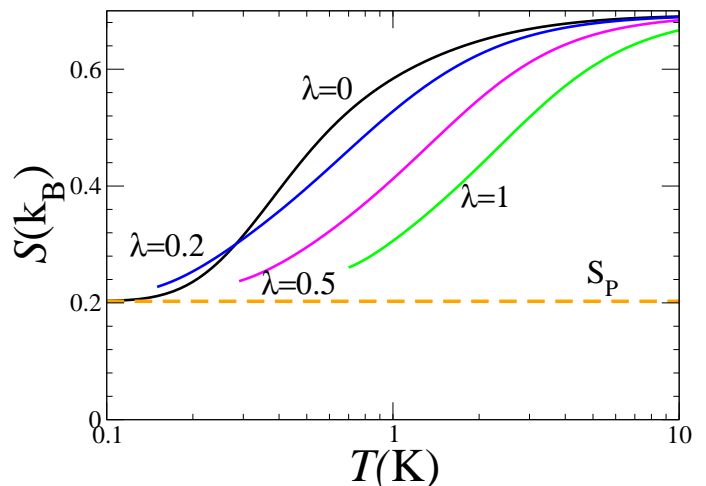


FIG. 8: S4: Entropy of the system, when quantum terms are scaled by λ . The orange line is the Pauling entropy S_P .

shown in Fig. S5. Note that while the models with different λ always have a short-range order peak, in the $J_1 - J_3$ model, long-range order temperature increases well past the short-range order peak with increasing J_3/J_1 .

Comparison of the experimental entropy vs NLC results

The entropy difference, $S(T_2) - S(T_1)$ between two temperatures T_1 and T_2 can be obtained by integrating

$C(T)/T$ between those two temperatures:

$$S(T_2) - S(T_1) = \int_{T_1}^{T_2} \frac{C(T)}{T} dT$$

The number of experimental specific heat, $C(T)$, results on $\text{Yb}_2\text{Ti}_2\text{O}_7$ has rapidly accumulated over the past year or so [19–21]. Most of these data are somewhat problematic in wanting to assess whether those thermodynamic data hide spin ice phenomenology, associated with a rapid diminution of spinon/antispinon excitation and the concurrent $C(T)$ hump at a temperature ~ 2 K as we now discuss.

All of the published $C(T)$ data [19–21, 27] do not go to sufficiently high temperature to extract reliably the limiting $C(T) \propto 1/T^2$ high temperature behaviour that would allow one to determine the residual magnetic entropy by integrating $C(T)/T$ upon decreasing T starting from the infinite $k_B \ln(2)$ value. One must therefore integrate $C(T)/T$ from low temperature, and assume an entropy value, S_{low} at some reference (low) temperature, T_{low} . The apparent large amount of residual entropy below ~ 0.2 K in the single crystal samples of Refs. [19–21] make difficult ascribing a reasonable value to S_{low} . This problem is further compounded by the rising low-temperature nuclear contribution to the total specific heat below about 0.1 K. The very sharp 1st order transition seen in powder powder sample of Ref. [20], without a precise measurement of the associated latent heat also make difficult using those data for comparison of experimental entropy with the $S(T)$ calculated by NLC. On the otherhand, the data of Blöte *et al.* [27] seem the most adequate for comparison with NLC: there is a sharp specific heat peak at $T_c \sim 0.24$ K with sufficient temperature resolution that allows integration of $C(T)/T$ over the peak without concern about an associated latent heat. The $C(T)$ data are dropping rapidly below T_c , suggesting the opening of an excitation gap, ultimately reaching a low-value that is limited by the “high temperature tail” ($T \sim 0.1$ K) of the nuclear contribution. Using the data from Ref. [27], we thus assume that the magnetic part of the specific heat is zero at $T = 0.1$ K, and integrate *upward* (increasing temperature) $C(T)/T$ up to the highest temperature point available from those data (~ 3.5 K). This results in the data (filled black circles in Fig. 3 in the body of the paper).

It would be highly desirable to repeat this procedure from the $C(T)$ data of Refs. [19–21] which show a sharp peak, but including (magnetic specific heat) data for T up to 20 K where the limiting high-temperature regime $C(T) \approx \frac{A}{T^2} + \frac{B}{T^3}$ can be fitted and compared with NLC, along with measurements of the magnetic entropy, $S(T)$.

limit available dataThe data from Working from the reasonable presumption high temperature

Monte Carlo Simulation of the $J_{zz} - J_3$ Model

In the perturbative regime of the QSI, we consider the effective Hamiltonian

$$\mathcal{H} = \sum_{\langle i,j \rangle} J_{zz} \sigma_i \sigma_j + \sum_{\langle i,j \rangle'} J_3 \sigma_i \sigma_j \quad (8)$$

where $\sigma = \pm 1$ are the Ising variables. $\langle \dots \rangle$ denotes the sum over the nearest neighbors, $\langle \dots \rangle'$ denotes the sum over the third nearest neighbors which share a nearest neighbour. Distance-wise there exists another type of third nearest neighbors which do not share a nearest neighbor. For any given spin, there are six third nearest neighbors for both types. Antiferromagnetic $J_{zz} > 0$ drives the spin ice formation in the classical spin ice system, and a small fluctuation-induced ferromagnetic exchange $J_3 \equiv -3J_{z\pm}^2/J_{zz} < 0$ favors the $\mathbf{q} = 0$ ordering within the spin ice manifold, *i.e.*, all tetrahedra on the same primitive FCC lattice have the same one of the six spin ice states.

Monte Carlo simulations are performed using the Metropolis algorithm. Single spin flip updates are used along with the non-local loop algorithm [37], which restores the ergodicity of the system once it is frozen into the spin ice states. Systems of 128 spins are simulated in a cubic box with periodic boundary conditions. Up to about 78,000 Monte Carlo steps per spin are used in equilibrating the system at a given temperature, with the same number of steps in data sampling. To investigate the calorimetric quantities, fluctuations of the energy are recorded to give the heat capacity:

$$C = \frac{\langle E^2 \rangle - \langle E \rangle^2}{k_B T^2} \quad (9)$$

Calculation of Monopole density

The defect (spinon/antispinon) monopole number $M(T)$, for a cluster, is evaluated as

$$\begin{aligned} M(T) &= \text{tr}(\hat{m} e^{-\beta \hat{H}}) / Z \\ &= \frac{1}{Z} \sum_{\alpha} e^{-\beta E_{\alpha}} \langle \alpha | \hat{m} | \alpha \rangle \\ &= \frac{1}{Z} \sum_{\alpha, k} e^{-\beta E_{\alpha}} |\langle \alpha | k \rangle|^2 m_k \end{aligned} \quad (10)$$

where m_k is the monopole count in the local S_z basis state $|k\rangle$. This count is a sum over all the tetrahedra in a cluster, $m_k = \sum_i m_{ki}$, where

$$m_{ki} = \begin{cases} 2 & \text{all in/out,} \\ 1 & \text{three in/out and one out/in,} \\ 0 & \text{two in and two out.} \end{cases} \quad (11)$$

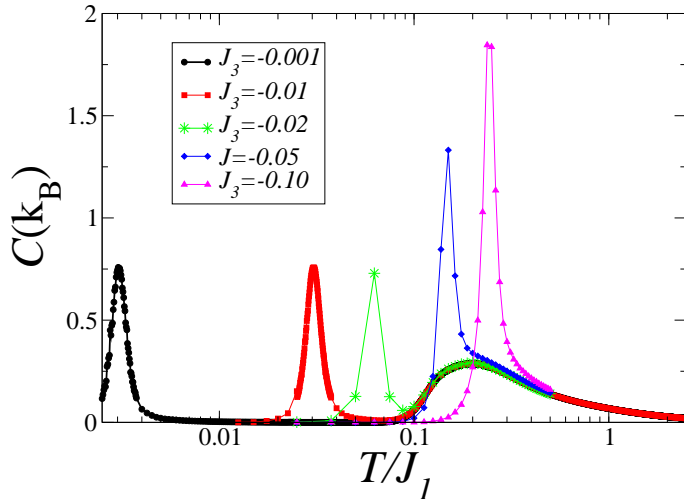


FIG. 9: S5: Heat capacity of the classical $J_{zz} - J_3$ model, with different J_{zz}/J_1 ratios.

The monopole density $\rho(T)$ is defined as number of monopoles present per site, giving

$$\rho(T) = M(T)/N. \quad (12)$$

-
- [1] L. Balents, *Nature* **464**, 199 (2010).
[2] M. J. P. Gingras, in *Introduction to Frustrated Magnetism*, (Springer, 2011) arXiv:0903.2772 .
[3] H. R. Molavian *et al.*, *Phys. Rev. Lett.* **98**, 157204 (2007).
[4] S. Onoda and Y. Tanaka, *Phys. Rev. Lett.* **105**, 047201 (2010).
[5] J. S. Gardner *et al.*, *Rev. Mod. Phys.* **82**, 53 (2010).
[6] L. Pauling, *J. Am. Chem. Soc.* **57**, 2680 (1935).
[7] W. F. Giaque and J. W. Stout, *J. Am. Chem. Soc.* **58**, 1144 (1936).
[8] A. P. Ramirez *et al.*, *Nature* **399**, 333 (1999); A. L. Cornelius and J. S. Gardner, *Phys. Rev. B* **64**, 060406 (2001).
[9] M. Hermele *et al.*, *Phys. Rev. B* **69**, 064404 (2004).
[10] A. H. Castro Neto *et al.*, *Phys. Rev. B* **74**, 024302 (2006).
[11] To relate our presentation more directly to the compact lattice QED context set in Refs. [9, 10], in which con-

finement in three-dimensions is traditionally referred to the strong (electric charge) coupling, we refrain from using the language of “monopoles” employed in Ref. [12] to label local defects in the ice rule of the parent classical spin ice. We use instead the more traditional wording of spinon/antispinon to label finite energy excitations out of the 2in/2out spin ice manifold.

- [12] C. Castelnovo *et al.*, *Nature* **451**, 42 (2008).
[13] A. Banerjee *et al.*, *Phys. Rev. Lett.* **100**, 047208 (2008); N. Shannon *et al.*, *ibid* **108**, 067204 (2012).
[14] J. A. Hodges *et al.*, *Phys. Rev. Lett.* **88**, 077204 (2002).
[15] K. A. Ross *et al.*, *Phys. Rev. Lett.* **103**, 227202 (2009).
[16] H. B. Cao *et al.*, *J. Phys. Condens. Matter* **21**, 492202 (2009).
[17] J. D. Thompson *et al.*, *Phys. Rev. Lett.* **106**, 187202 (2011).
[18] K. A. Ross *et al.*, *Phys. Rev. X* **1**, 021002 (2011).
[19] A. Yaouanc *et al.*, *Phys. Rev. B* **84**, 172408 (2011).
[20] K. A. Ross *et al.*, *Phys. Rev. B* **84**, 174442 (2011).
[21] L.-J. Chang *et al.*, arXiv:1111.5406
[22] B. Z. Malkin *et al.*, *J. Phys. Cond. Matter* **22**, 276003 (2010).
[23] S. Onoda, *J. Phys.: Conf. Series.*, **320**, 012065 (2011).
[24] J. D. Thompson *et al.*, *J. Phys. Condens. Matter* **23**, 164219 (2011).
[25] L. Savary and L. Balents, *Phys. Rev. Lett.* **108**, 037202 (2012)
[26] Y. Wan and O. Tchernyshyov, arXiv:1201.5314
[27] H. W. J. Blöte *et al.*, *Physica* **43**, 549 (1969).
[28] Y. Yasui *et al.*, *J. Phys. Soc. Jpn.* **72**, 3014 (2003).
[29] J. S. Gardner *et al.*, *Phys. Rev. B* **70**, 180404(R) (2004).
[30] J. Oitmaa, C. Hamer and W. Zheng, *Series Expansion Methods for strongly interacting lattice models* (Cambridge University Press, 2006).
[31] M. Rigol *et al.*, *Phys. Rev. Lett.* **97**, 187202 (2006); *Phys. Rev. E* **75**, 061118 (2007); *Phys. Rev. E* **75**, 061119 (2007).
[32] See Supplementary Material.
[33] R. R. P. Singh and J. Oitmaa, arXiv:1112.4439.
[34] See for example, *Numerical Recipes*, by W. H. Press *et al.*, Cambridge University Press (1989), Page 133.
[35] These are geometrically 3rd neighbors on the pyrochlore lattice but not all 3rd neighbors belong to this category.
[36] C. L. Henley, *Annu. Rev. Cond. Matt. Phys.* **1**, 179 (2010).
[37] R. G. Melko and M. J. P. Gingras, *J. Phys.: Condens. Matter* **16**, R1277 (2004).
[38] V. Elser, *Phys. Rev. Lett.* **62**, 2405 (1989). N. Elstner and A. P. Young, *Phys. Rev. B* **50**, 6871 (1994).